PROCEEDINGS, 42nd Workshop on Geothermal Reservoir Engineering
Stanford University, Stanford, California, February 13-15, 2017
SGP-TR-212

High-Resolution Subsurface Imaging at Soda Lake Geothermal Field

Kai Gao, Lianjie Huang

Geophysics Group, Los Alamos National Laboratory, Los Alamos, NM 87545

kaigao@lanl.gov, ljh@lanl.gov

Keywords: fault, fracture, full-waveform inversion, reverse-time migration, Soda Lake, subsurface imaging.

ABSTRACT

Accurate subsurface velocity models and structural images are of great importance for geothermal reservoir characterization, particularly for fault/fracture detection. However, complex faults/fracture zones in geothermal systems introduce great challenges to reliable estimation of subsurface velocity models and clear imaging of complicated geological structures. We develop a novel multiscale, correlative full-waveform inversion method, and apply the method to 3D seismic data acquired at Soda Lake geothermal site to build a high-resolution 3D velocity model. The inverted velocity model shows some fine geological features with velocity values lower than those of surrounding media. These features may be associated with fault/fracture zones. To obtain a high-resolution subsurface image of Soda Lake geothermal field, we conduct reverse-time migration using 3D compressional-wave and compression-to-shear converted-wave data and the inverted 3D velocity model. Our results demonstrate that 3D full-waveform inversion significantly improves subsurface images of 3D reverse-time migration. We find that the low velocity zones in our velocity inversion results are mostly located along the fault/fracture zones shown in our reverse-time migration images. These high-resolution imaging results could guide the optimal placement of hydrothermal production wells.

1. INTRODUCTION

The Soda Lake geothermal field is located in the south central part of the Carson Sink (Figure 1), about six miles northwest of the town of Fallon. It is surrounded by other operating geothermal fields such as Desert Peak, Bradys, Stillwater and Salt Wells. Explorations of geothermal resources dated back to 1971 by the U.S. Geological Survey, followed by drilling activities in late 1970s and early 1980s by Chevron and Phillips. The most recent geothermal exploration activity was conducted by Magma Energy Corp from 2008 to 2010.

The Soda Lake geothermal field lies directly between the over 10,000 year-old Big Soda Lake volcanic explosion crater, and the mafic Quaternary Upsal Hogback volcanic complex. From the surface to depths of 1550 feet to 1800 feet, the geology consists of layered unconsolidated Quaternary and possibly Pleistocene sediments deposited as part of the Carson River delta and Lake Lahontan mud (Morrison, 1964; Sibbett, 1979). Based on the well log correlations and interpretations by Magma Energy Corp., the top of a very prominent basaltic unit could be delineated between the depths of 1470 feet and 2190 feet. Most of the normal faults interpreted from the time migration images appear to be in the NE-SW strikes and with steep dips, complicating the permeability environment for geothermal fluid flows. The Soda Lake shallow thermal anomaly reaches to a depth of 500 feet, defining a roughly circular area of 30 to 35 square miles. Temperatures from 69°F to 338°F were measured at a depth of 500 ft. Temperature gradients above a depth of 500 feet range from a background of about 3°F/100 feet to extreme values in the center of the anomaly that cannot be extrapolated to greater depths (Magma Energy Soda Lake DOE Phase I Report, 2011).

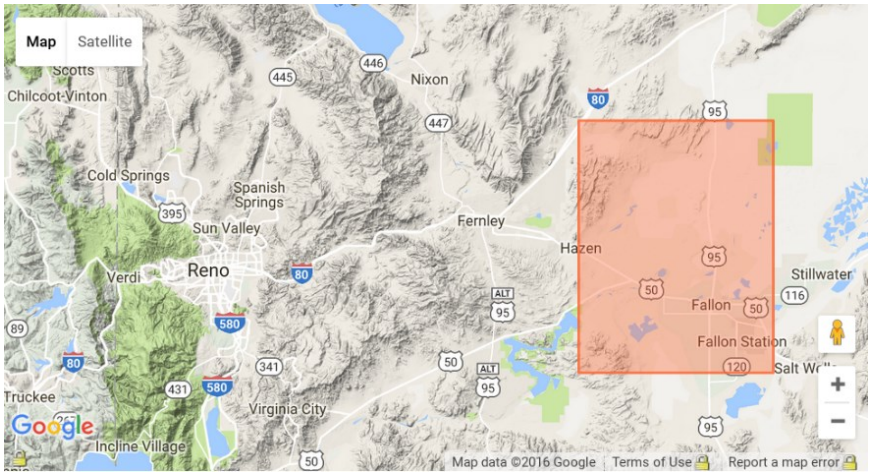

Figure 1: Geographical location of Soda Lake geothermal field. The image is snapshotted from Google Map.

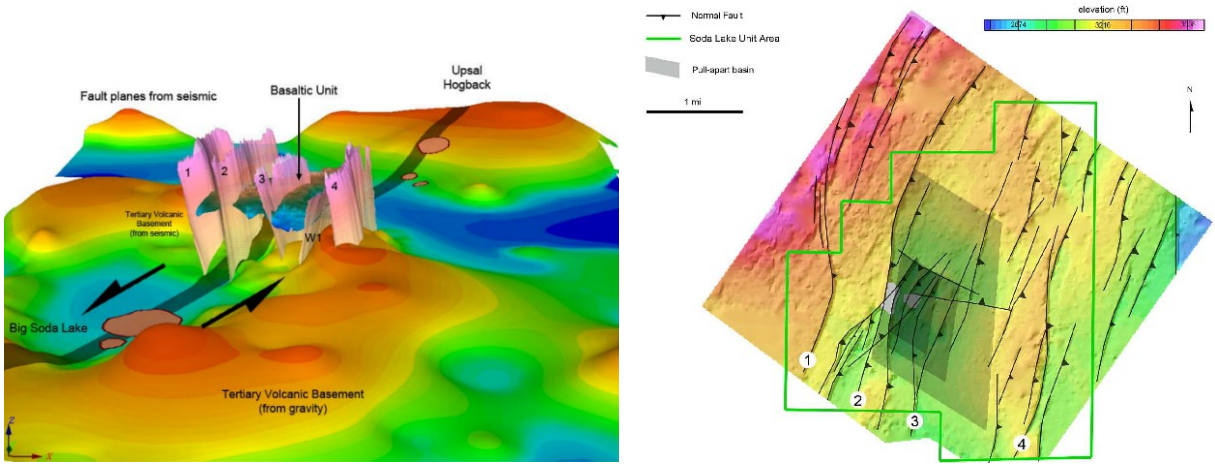

(a) (b)

Figure 2: (a) Conceptual geological model showing major stratigraphy units and faults at Soda Lake geothermal field. (b) Structure map showing normal faults (indicated by arrowed block curves). The images are part of the interpretation results from Magma Energy Corp's Soda Lake DOE Phase I Report on Soda Lake 3D-3C reflection seismic survey.

In this study, we aim to build accurate subsurface velocity models and high-resolution structural images using the acquired surface seismic data, which are of great importance for geothermal reservoir characterization, particularly for fault/fracture detection. However, complex faults/fracture zones in Soda Lake geothermal systems introduce great challenges to reliable estimation of subsurface velocity models and clear imaging of complicated geological structures. To address these challenges, we develop a multiscale, correlative full-waveform inversion (FWI) algorithm for high-resolution velocity model building based on an existing smooth velocity model derived from migration velocity analysis. In addition, we apply our newly developed reverse-time migration (RTM) algorithm based on implicit wavefield-separation imaging condition to produce clear subsurface structural images. We describe our methodology and present some seismic inversion and imaging results in the following Methodology and Results sections.

2. METHODOLOGY

Conventional seismic data processing techniques, such as normal moveout correction-based velocity analysis and migration velocity analysis, can provide spatially smooth velocity models with satisfactory traveltime information. However, these models usually lack sufficient resolution for fault/fracture zones interpretation and characterization. To build accurate velocity models and produce high-resolution subsurface images, we develop and apply a multiscale, correlative FWI and a RTM method based on implicit wavefield separation imaging conditions.

2.1 Multiscale, correlative FWI

FWI is a nonlinear minimization method for estimating subsurface medium properties by minimizing the misfit functional between the observed data and the numerical synthetic data (e.g., Tarantola, 1984):

$$\chi(m) = \sum_{N_s, N_r} \| d - f(m) \|_2^2 , \tag{1}$$

where d is an observed seismic waveform, $f(m)$ is a numerical synthetic seismic waveform, and m represents the model, which can be P- or S-wave velocity, or elasticity parameters. However, various interfering factors can prevent us from reliably matching between synthetic data and field data. These factors include but are not excluded to ambient noises, imperfect receiver-medium coupling, simplified Earth medium assumptions, inaccuracies of wavelet estimation, etc. These interferences pose severe difficulties to FWI based on the data misfit functional in Equation (1) that uses absolute data differences as the data matching criterion.

We develop a correlative misfit functional for FWI to alleviate the aforementioned data matching problem:

$$\chi_{\text{corr}}(m) = \sum_{N_s, N_r} \left[1 - \frac{d}{\sqrt{\int_0^T |d|^2 \, dt}} \frac{f(m)}{\sqrt{\int_0^T |f(m)|^2 \, dt}} \right] . \tag{2}$$

That is, observed data and synthetic data are first normalized with the square root of their respective wave energy before the misfit is computed. Equation (2) represents the correlative difference between synthetic data and observed data. For a certain seismic trace, if the

synthetic and observed waveforms are perfectly matched, the misfit reduces to zero as in conventional FWI; if the observed and the synthetic waveforms differ from a constant scaling factor for a certain seismic trace, the misfit still reduces to zero, resulting in a robust matching criterion for FWI. This misfit criterion is particularly useful for field data applications, where the absolute data matching might never be possible. The FWI gradient using Equation (2) as the misfit functional can be computed using the adjoint-state method (e.g., Plessix, 2006), but with a different residual data term as the adjoint source compared with that based on Equation (1).

2.2 RTM based on wavefield separation imaging conditions

RTM is an accurate and effective technique for complex subsurface structure imaging, posing no limitations in structure dipping angles (McMechan, 1983). To form subsurface structural images, conventional RTM uses zero time lag cross-correlation between the source and the receiver wavefields:

$$I(x) = \sum_{N_s, N_r} \int_0^T S(x,t) R(x,t) dt \ , \tag{3}$$

where $S(x,t)$ is the source wavefield and $R(x,t)$ is the receiver wavefield. Studies show that the imaging condition in equation (1) contains low wavenumber artifacts resulting from the cross-correlation between the wavefields propagating in the same direction (Liu et al., 2011). In addition, the imaging condition in Equation (1) cannot distinguish the images dominated with horizontally-dipping structures (sedimentary layers) and that dominated with vertically-dipping structures (faults and fractures). We employ RTM imaging conditions based on implicit wavefield separation (Fei et al., 2015):

$$\begin{aligned}
I_{\text{down}}(x) &= \sum_{N_s, N_r} \int_0^T SR - H_z(S) H_z(R) - S H_z(H_t(R)) - H_z(S) H_t(R) dt \\
I_{\text{right}}(x) &= \sum_{N_s, N_r} \int_0^T SR - H_x(S) H_x(R) - S H_x(H_t(R)) - H_x(S) H_t(R) dt \ , \\
I_{\text{back}}(x) &= \sum_{N_s, N_r} \int_0^T SR - H_y(S) H_y(R) - S H_y(H_t(R)) - H_y(S) H_t(R) dt
\end{aligned} \tag{4}$$

where H_t represents the Hilbert transform in the time domain, and H_x, H_y and H_z represent the Hilbert transforms in the x, y and z direction, respectively. I_{down}, I_{right} and I_{back} are the down-going, right-going and back-going images, respectively. RTM images for other axis directions (e.g., left-going or front-going) can be written in similar formulations.

3. RESULTS

We conduct 3D full-waveform inversion and 3D reverse-time migration imaging using 3D surface seismic data acquired at Soda Lake geothermal site. The seismic data are processed using several different procedures to eliminate random noises and surface-related noises. Surface consistent processing is also applied to the data, including static corrections and surface-consistent amplitude corrections using frequency-space domain filters. In addition, an initial depth-domain velocity model is built using migration velocity analysis.

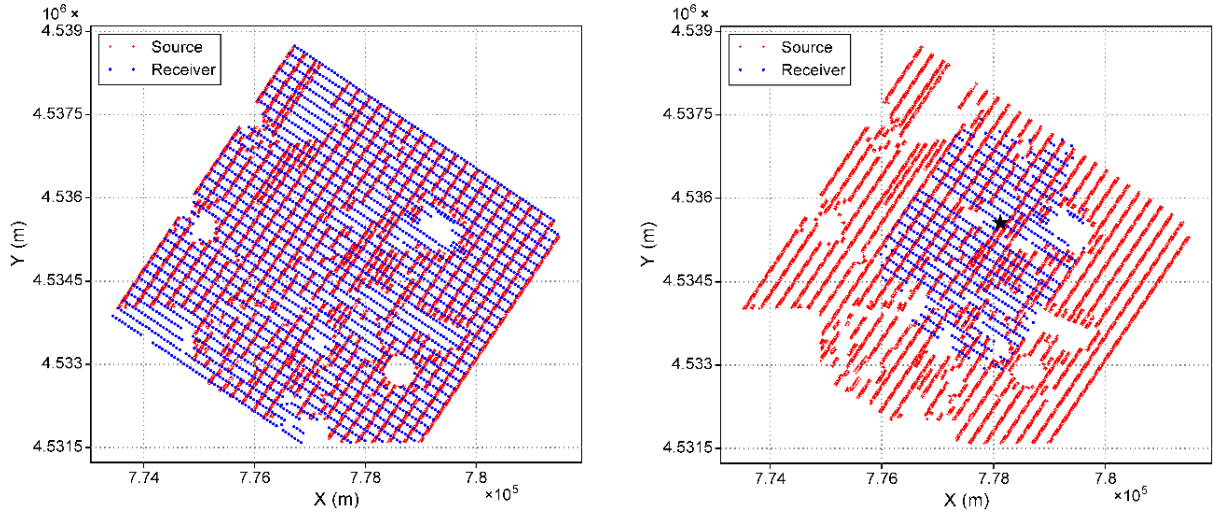

Figure 3: (a) Source and receiver distribution for 3D surface seismic survey at Soda Lake geothermal field. Red dots represent source positions, blue dots denote receiver points. (b) Plot of an example common-shot gather with blue dots representing receiver locations and black star denoting source positions.

The first procedure for conducting FWI and RTM is the extraction and setup of the appropriate source-receiver geometry. The geometry is extracted using our in-house SEG-Y data I/O utility. Figure 3(a) shows the distribution of sources and receivers for the 3D surface seismic survey at Soda Lake geothermal field, and Figure 3(b) displays the source-receiver geometry of an example common-shot gather. The source lines are in SW-NE direction with a line interval of 235.5 meters. The receiver lines are in NW-SE direction with a line interval of 167.5 meters. The receiver interval is 67 meters and the shot interval is 33.5 meters. The azimuth of the source lines is 33.97 degrees. Before proceeding to FWI or RTM, we rotate the geometry to regular coordinates, i.e., with zero degree azimuth, a step to ensure the consistency between the regular-gridded model and geometry. In addition, we shift the coordinates of the source-receiver geometry with appropriate constants for both X and Y, i.e., along E-W and N-S directions.

A total of 8317 common-shot gathers were acquired to cover the whole survey area. The number of receivers in each common-shot gather varies from several hundreds to more than one thousand. Both FWI and RTM are time-consuming tasks, and the computation costs are directly proportional to the number of discrete grids for the heterogeneous model and the number of seismic shots. Therefore, we transform the common-shot gathers to a total of 2972 common-receiver gathers to reduce computation costs.

Figure 4 shows an example common-receiver gather extracted for our inversion and imaging tasks. We apply frequency bandpass filtering and data resampling to the extracted common-receiver gather to facilitate our subsequent inversion and imaging. For multiscale FWI, we bandpass filter the data several times with different selective frequency bands. A careful bandpass filtering is also helpful in reducing noises in the seismic data. We also balance seismic traces to enhance reflection events throughout the common-receiver gathers. This balancing also helps reduce the amplitude of remaining ground roll noises in the processed seismic data.

For RTM imaging, a wide frequency band enhances the image resolution. Seismic data with time-variant spectral whitening are therefore used for our RTM imaging.

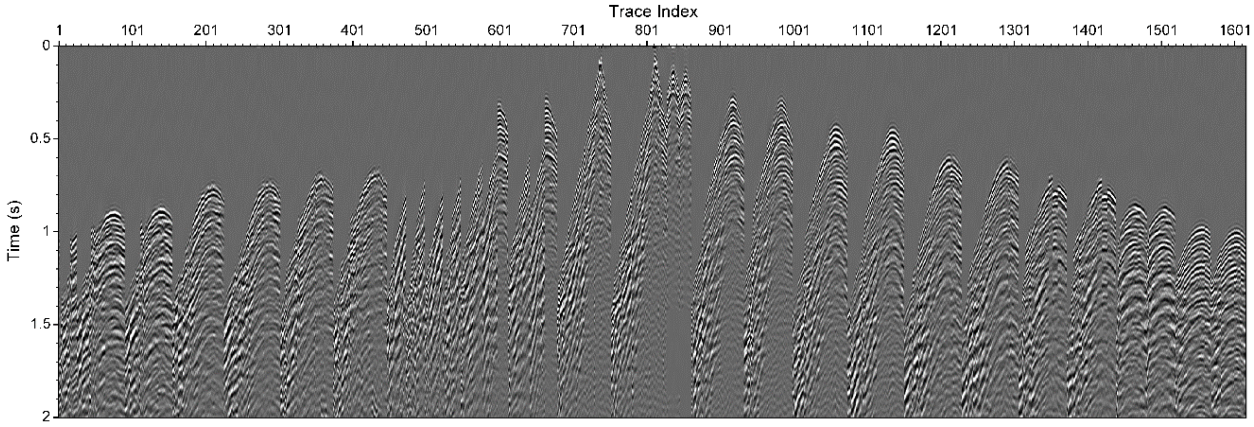

Figure 4: An example common-receiver gather extracted from the processed seismic data acquired at Soda Lake geothermal field.

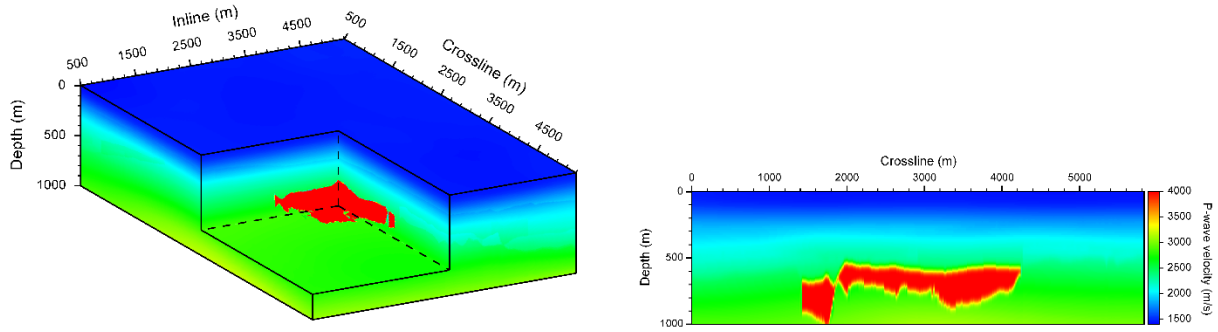

(a) (b)

Figure 5: (a) A 3D view of the initial P-wave velocity model built using migration velocity analysis, and (b) a 2D crossline slice of the initial velocity model.

An accurate initial velocity model is essential for successful FWI. The initial velocity model used in our multiscale FWI is built using migration velocity analysis. The sole clear reflector in this initial velocity model is the boundary of the high-velocity basalt unit, a feature consistent with Magma Energy Corp's studies. Figure 5(a) shows a 3D view of the initial P-wave velocity model, and Figure 5(b) depicts a crossline 2D slice of the initial model.

We apply the aforementioned multiscale, correlative FWI to build a high-resolution velocity model. Starting from low frequencies up to 10 Hz, we gradually widen the frequency band to include higher frequency seismic signals to invert for finer structures. Figure 6(a) displays a 3D view of the inverted 3D velocity model. Figure 6(b) shows the inverted P-wave velocity model on a 2D crossline. Several low-velocity zones (pointed by the black arrows in Figure 5b) can be observed in the inverted velocity model. These low-velocity zones are very likely associated with the faults and fracture zones indicated in the aforementioned conceptual geological models (Figure 2a) and the fault map (Figure 2b).

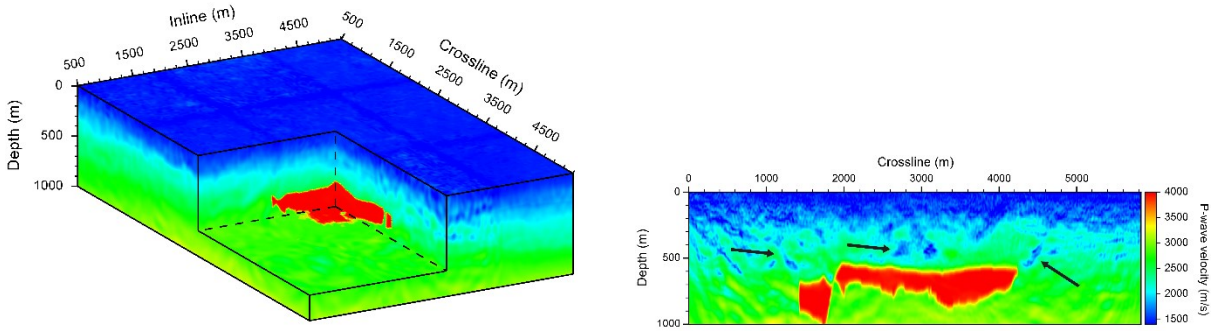

(a) (b)

Figure 6: (a) A 3D view of the inverted P-wave velocity model, and (b) a 2D crossline slice of the inverted velocity model, obtained using full-waveform inversion of 3D surface seismic data acquired at Soda Lake geothermal field.

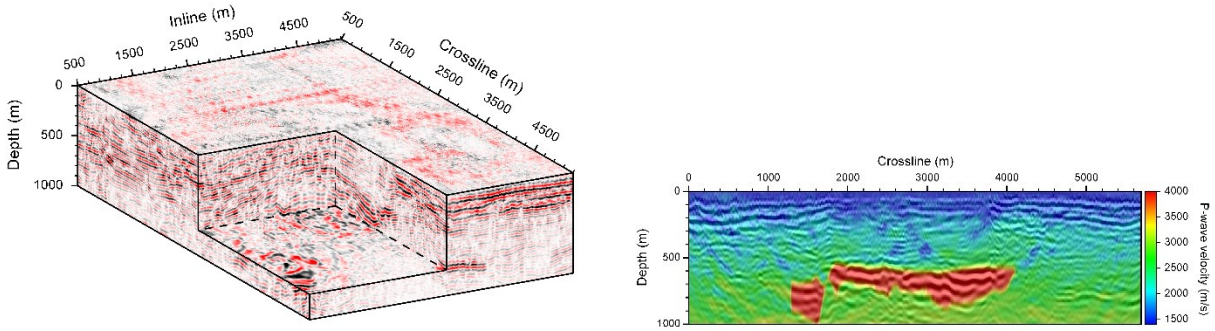

(a) (b)

Figure 7: (a) A 3D view of the PP image of Soda Lake geothermal field obtained using RTM with the wavefield-separation imaging condition, and (b) a 2D crossline slice of the PP image overlying on the FWI inverted P-wave velocity model.

Figure 7(a) shows the 3D PP image obtained with our implicit wavefield-separation-based RTM method. Near surface sedimentary layers are imaged clearly. In Figure 7(b), a 2D crossline slice of the RTM image overlies on the velocity model inverted with FWI. At the low-velocity regions indicated by arrows in Figure 6(b), the reflectors are less continuous, indicating the consistency between the FWI inverted velocity model and the RTM image. These results can guide the optimal placement of hydrothermal production wells. In addition, we perform converted-wave RTM using PS converted-wave seismic data, and the imaging results are shown in Figure 8(a) and Figure 8(b). The top of the basalt unit is clearly delineated in both the PP and PS images.

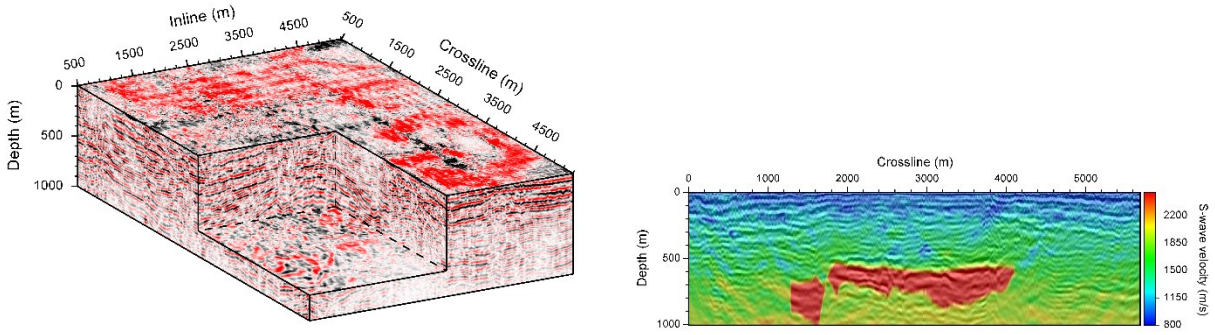

(a) (b)

Figure 8: (a) A 3D view of the PS image of Soda Lake geothermal field obtained using RTM with the wavefield-separation imaging condition, and (b) a 2D crossline slice of PS image overlying on the FWI inverted S-wave velocity model.

4. CONCLUSIONS

We have conducted 3D full-waveform inversion and 3D reverse-time migration of 3D surface seismic data acquired at Soda Lake geothermal field, and obtained high-resolution velocity models and subsurface geological structure images. For high-resolution velocity model building, we have developed and applied a multiscale, correlative full-waveform inversion method to the data. To image faults and fracture zones, we have developed and applied an efficient reverse-time migration algorithm based on implicit wavefield separation to the 3D seismic data. The low velocity zones in full-waveform inversion results are consistent with migration images, and they may be associated with fault/fracture zones at Soda Lake geothermal field.

5. ACKNOWLEDGEMENTS

This work was supported by the Geothermal Technologies Office (GTO) of the U.S. Department of Energy through contract DE-AC52-06NA25396 to Los Alamos National Laboratory. We thank strong support of GTO Program Managers Eric Hass, Mark Ziegenbein, Holly Thomas, and Brittany Segneri. The computation was performed on super-computers provided by the Institutional Computing Program of Los Alamos National Laboratory.

REFERENCES

Fei, T. W., Luo, Y., Yang, J., Liu, H., and Qin, F.: Removing false images in reverse time migration: The concept of de-primary, *Geophysics*, **80**, (2015), S237-S244.

Liu, F., Zhang, G., Morton, S. A., and Leveille, J. P.: An effective imaging condition for reverse-time migration using wavefield decomposition, *Geophysics*, **76**, (2011), S29-S39.

Magma Energy Corp: Soda Lake DOE Phase I Report: Soda Lake 3D-3C Reflection Seismic Survey, (2011).

McMechan, G. A.: Migration by extrapolation of time-dependent boundary values, *Geophysical Prospecting*, **31**, (1983), 413-420.

Morrison, R. B: Lake Lahontan: geology of southern Carson desert, Nevada, U. S. Geological Survey, Prof. Paper 401, (1964).

Plessix, R.-E.: A review of the adjoint-state method for computing the gradient of a functional with geophysical applications, *Geophysical Journal International*, **167**, (2006), 495-503.

Sibbett, B. S.: Geology of the Soda Lake geothermal area, Earth Sciences Laboratory, University of Utah Research Institute, Publication DOE/ET 283293-34 78-1701.b.1.2.3 ESL-24, (1979).

Tarantola, A.: Inversion of seismic reflection data in the acoustic approximation, *Geophysics*, **49**, (1984), 1259-1266.